Metals and Materials International (2022) 28:456–465
https://doi.org/10.1007/s12540-021-01075-7

Solidification Structure Evolution and Grain Refinement Mechanism of a Deeply Undercooled Ni65Cu35 Alloy

Xiaolong Xu[1] · Yukang An[1] · Hua Hou[1] · Yuhong Zhao[1]

Received: 1 November 2020 / Accepted: 13 June 2021 / Published online: 29 October 2021

Abstract
The maximum 320 K undercooling of Ni65Cu35 alloy was obtained by means of cyclic superheating in the state of molten glass. The solidification structuresat different undercoolings were systematically studied. There are two grain refinementsat low and high undercoolings. It was generally believed that the grain refinement atlowundercooling was caused by dendrite superheat remelting. Electron backscattering diffraction was used to characterize the solidification structure athighundercooling, and obvious random orientation, high-angle grain boundaries and twin boundaries were found, indicating grain refinement was caused by recrystallization under highundercooling. There were almost no visible dislocation defects in the TEM bright-field images at high undercooling, and the microstructure hardness decreased obviously after grain refinement. This further illustrated the rapid accumulation of stress and defects in recalescenceare completely abreacted in recrystallization during post-recalescence period, at the same time as the driving force to promote the second grain refinement in the microstructure.

Keywords Undercooling · Grain refinement · Recalescence · Recrystallization

1 Introduction

Under the influence of grain refinement, the structure and properties of metal materials will change greatly, and the main actor is reflected in strength, plasticity, toughness and other properties [1–3]. Studies [1] on grain refinement of materials can be traced back to the deep undercooling rapid solidification experiment of nickel melt by Walker. Since the deep undercooling experiment of nickel melt, the phenomenon of grain refinement in undercooled alloys or metals and the mechanism of grain refinement have been studied systematically [4–13]. At the microscopic level, metal solidification occurs when atoms attach to impurities. The melting glass purification method, falling tube method, cyclic overheating method and electromagnetic suspension smelting method can be used to remove impurities in the metal melt to the greatest extent, prevent heterogeneous nucleation, and make the metal melt nucleate and grow at a lower temperature, so as to obtain a greater degree of undercooling [7, 14, 15]. Batters by obtained the undercooling degree of 300 K for Ge and Ge-Fe by using the molten glass purification method, and studied the relationship between the rapid solidification rate of deep undercooling and the undercooling degree. Li [16–25] studied the rapid solidification process of the entire deeply undercooling Ni-Cu alloy system, and found that Ni-Cu alloys had grain refinement phenomenaat both low and high undercoolings, but the microstructure of grain refinement was very different between the two refinements.

Although there were two grain refinements in different undercooling ranges, the structured morphologies of the two grain refinements were completely different, which indicated that the formation mechanisms of the two phenomena were different. Various mechanisms [19, 26–30] have been proposed to explain this phenomenon, such as dendrite remelting mechanism, critical velocity theory, dynamic nucleation, recrystallization and so on. The grain refinementat the condition of low undercooling can be explained by the dendrite superheat remelting mechanism [7, 17, 31]. The latent heat of crystallization released during solidification makes the system temperature rise above the solidus, and the

✉ Xiaolong Xu
xiaolong4253@163.com

✉ Yuhong Zhao
zhaoyuhong@nuc.edu.cn

[1] College of Materials Science and Engineering, North University of China, Taiyuan 030051, Shanxi, China

primary dendritesare broken into fine equiaxed grains due to superheating. However, there is no established mechanism or theory to explain grain refinement at high undercooling. The dendrite remelting and dynamic nucleation are not consistent with the experimental results, and critical velocity theory cannot be verified for each alloy. Recently, the stress-induced recrystallization [32–36] has attracted much attention of researchers. With the increase of initial undercooling, the volume fraction of solid phase increases continuously, and the continuous dendrite network starts to form, so that the dendrite skeleton has deformation strength. At the same time, due to the solidification shrinkage, stress accumulation begins between the dendrite skeleton during rapid solidification. When the accumulated stress exceeds the yield strength of the alloy, dendrite fracture and plastic deformation occur, and the resulting plastic strain can be used as a driving force for subsequent recrystallization. However, for the alloys with high melting point, the recrystallization mechanism has not been fully recognized [7, 37]. Therefore, it is necessary to clarify the grain refinement mechanism of the alloy at high undercooling to better control the microstructure and properties of the alloy in non-equilibrium solidification. In this paper, the rapid solidification structure evolution of binary single-phase Ni65Cu35 alloy is systematically studied by means of melting glass purification combined with cyclic superheating. The grain orientation and grain boundaries characteristics of the two grain refinement structures at low and high undercoolings were observed by electron backscattering diffraction (EBSD). The structure of grain refinement under highundercooling was characterized by transmission electron microscope(TEM) and microhardness to further explain the stress-induced recrystallization mechanism.

2 Experimental Procedures

Ni65Cu35 parent alloy was prepared by proportional melting of pure nickel (99.99%) and pure copper (99.99%) in a vacuum arc melting furnace under the protection of high purity argon. In order to ensure the uniformity of alloy composition, the alloy was remelted at least 3 times in the melting furnace. Cut about 4 g sample for reserve. The alloy sample and quartz tube were cleaned with alcohol in the ultrasonic cleaner for about 10 min to achieve the preliminary purification effect. The cleaned alloy sample and a small amount of B_2O_3 are placed in a quartz tube mounted in a high-frequency induction coil. Vacuum up to 3×10^{-3}pa, argon backfill to 5×10^{-2} pa. The temperature change during rapid solidification was recorded with an infrared thermometer with response time of 1 ms. Firstly, the temperature is heated below the melting point of the alloy to fully melt B_2O_3 to cover the alloy. Then, the system temperature is heated to 150 to 250 K above the melting point for 20 min to fully absorb and decompose the impurities and minimize the heterogeneous nucleation. Then go through the thermal cycle and cooling until the ideal undercoolingsare obtained. The experimental principle of rapid solidification under deeply-undercooling is shown in Fig. 1.

The undercooled alloy samples were cut, embedded and polished, and then corroded in a mixture of 50%HCI and 50%HNO_3. The microstructure of the samples was observed with an optical microscope (Olympus GX71). Al_2O_3 colloidal suspension was used in vibration polishing machine to remove the surface stress layer of the sample. The grain orientation and grain boundary characteristics of the microstructure were observed by EBSD technology, and the microstructure at high undercooling was further characterized by TEM. On the microhardness tester (HMV-2 T), the microhardness of each sample was measured with a load of 490.3mN for a duration of 15 s. To ensure the uniformity of the measured results, at least 20 points are measured for each sample.

3 Results and Discussions

3.1 Solidification Microstructure Evolution

In order to obtain a higher undercooling of Ni65Cu35 alloy, the maximum 320 K undercooling of Ni65Cu35 alloy was obtained by melting glass purification and cyclic superheat. Infrared thermometer was used to record the temperature change during the whole rapid solidification process. The temperature curves of some typical undercoolings were shown in Fig. 2.

Figure 2 shows the solidification recalescence curves of Ni65Cu35 alloy at different undercoolings. The undercooling of the alloy is the difference between the liquidus temperature$T_L$and the nucleation temperatureT_N, which is shown in Fig. 2. The solidus and liquidus have been marked in Fig. 2. According to Fig. 2, with the increase of undercooling, the maximum recalescence temperatureT_R decreased gradually. When theT_R is lower than the solidus, the alloy can completely solidify during the recalescence, which we call the alloy to reach the hypercooling state [38]. According to Xu [14], the smaller the difference between the solidus and liquidus ($T_L^-T_S$), the easier to achieve hypercooling. Becausewhen the difference (T_L-T_S)is smaller, the solidus is higher and the temperatureT_R can easily be lower than the solidus, so the undercooling of the alloy in the hypercooling state is small. In Ni-Cu alloy system, when the atomic content of solute Cu is 30%–50%, the difference (T_LT_S) is larger and the solidus is lower, so the Ni65Cu35 alloy has a higher undercooling when it reaches the hypercooling state. It can be seen that when$\Delta T = 140$ K, the temperature$T_R$just reaches the solidus, indicating that the Ni65Cu35 reaches the

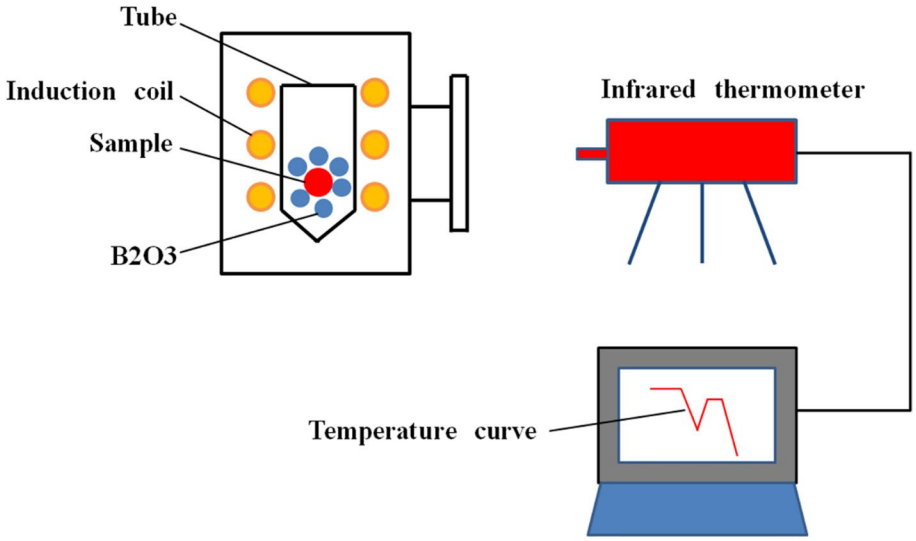

Fig. 1 Schematic diagram of deeply undercooling rapid solidification experimental facility

critical hypercooling state at this time. After exceeding the above critical hypercooling, the effect of dendrite remelting has disappeared (see$\Delta T = 200$ K), but a large number of hexagonal regular equiaxed grains appear in the microstructure, see Fig. 3g–h. It is obvious that the second grain refinement at high undercooling is not related to dendrite remelting. The latter part will further prove that grain refinement mechanism at high undercooling.

At low undercooling ($\Delta T = 45$ K and$\Delta T = 115$ K), the maximum recalescence temperatures T_R rise to above the solidus, the primary dendrites formed during rapid solidification will undergo remelting due to superheat, resulting in a large number of dendritic fragments and residual liquid phase. During post-recalescence period, the broken dendrite fragments float and collide in the residual liquid phase due to convection effect [39–41], and with the slow solidification of the residual liquid phase, the refined structures are finally formed due to resolidification, see Fig. 3b. This also shows that the grain refinement atlow undercooling is caused by dendrite superheat remelting.

There are two grain refinements in Ni65Cu35 alloy at different undercoolings. The evolution of solidification structure can be divided into four ranges:

(1) $\Delta T < 70$ K When the undercooling is very small, there are a large number of coarse dendrites in the microstructure without obvious growth orientation (Fig. 3a). The secondary dendritic arms surround the dendrites and the grain size is obviously larger than that the highundercooling. The BCT[6, 42]model indicates that the solute diffusion controls the dendrite growth in a narrow range at low undercooling, so the microstructure presents a coarse dendriticmorphology.

(2) 70 K $< \Delta T < 110$ K As the undercooling increases to this range, circular equiaxed grains increase gradually.

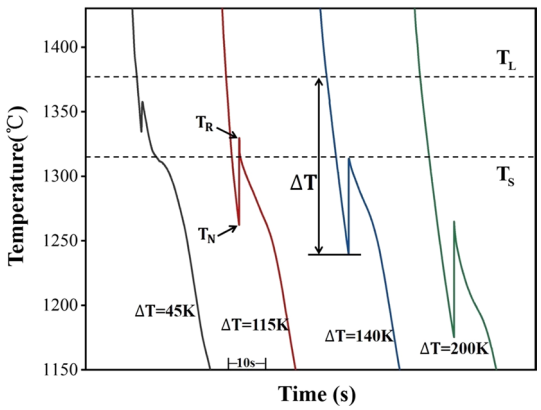

Fig. 2 Rapid solidification temperature curves of Ni65Cu35 alloy at different undercoolings

The first grain refinement occurs in the microstructure ($\Delta T = 70$ K, see Fig. 3b), and it ends at 110 K with the occur of directional fine dendrites (Fig. 3c).

(3) 110 K $< \Delta T < 195$ K With the increase of undercooling, the equiaxed grainsdisappear gradually, and a large number of fine dendrites can be seen, showing a developed fine dendritic network, see Fig. 3d–e. The primary dendritic skeleton can be seen clearly with similar growth orientation. This is due to the dominant role of thermal diffusion instead of solute diffusion, and the dendrite growth proceeds along the direction of thermal diffusion[37, 43].

(4) $\Delta T > 195$ K When the undercooling reaches the critical value ($\Delta T = 195$ K), it can be clearly seen that the primary dendritic skeleton is refining into equiaxed structure (Fig. 3f). This indicates that the second grain refinement begins to occur at $\Delta T = 195$ K. When $\Delta T > 195$ K, the microstructure is completely refined

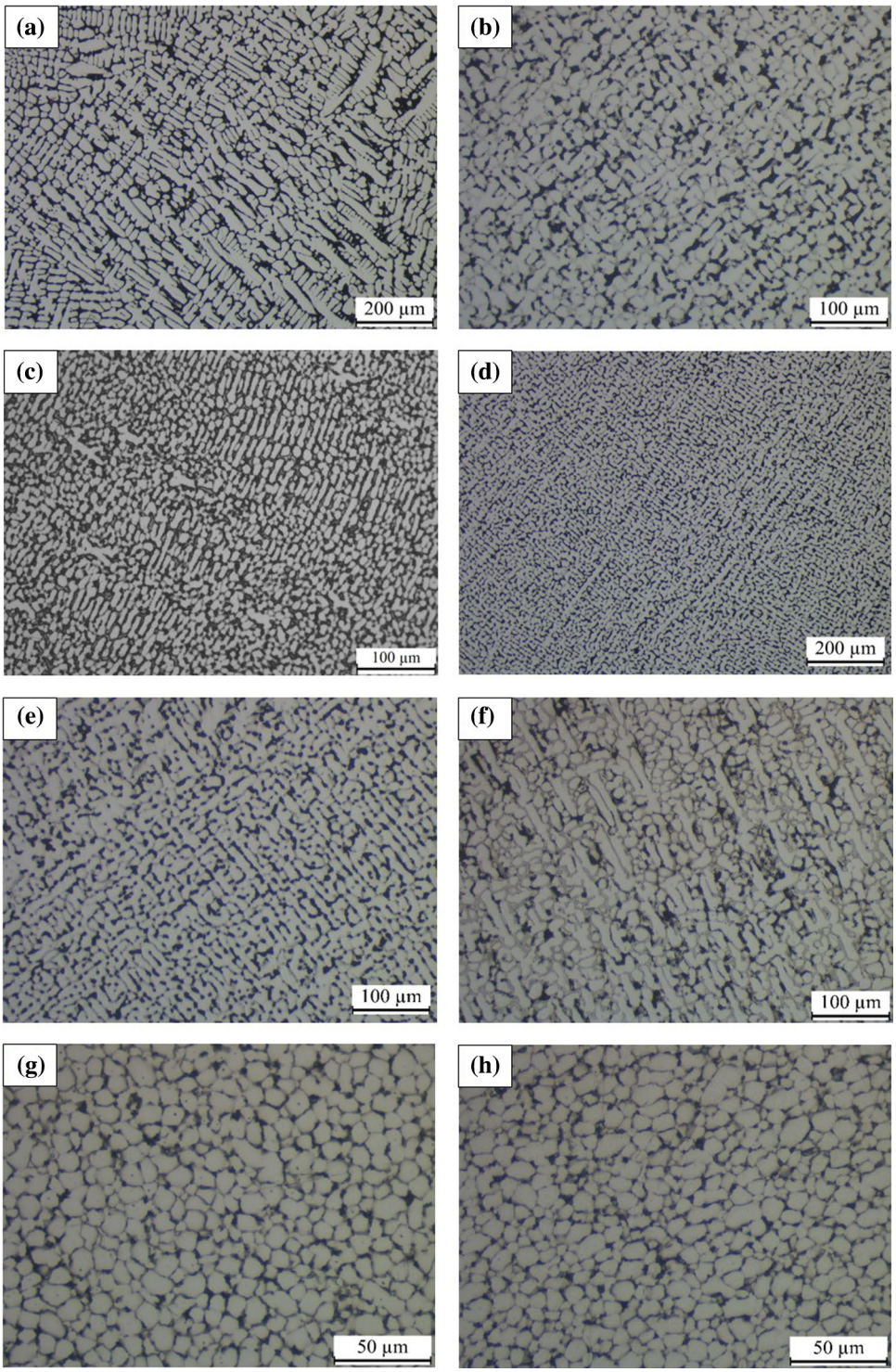

Fig. 3 Microstructure evolution of Ni65Cu35 alloy under different undercoolings (**a** 45 K; **b** 70 K; **c** 110 K; **d** 145 K; **e** 165 K; **f** 195 K; **g** 260 K; **h** 300 K)

equiaxed grained structure, and there is no dendritic structure, see Fig. 3g–h. This indicates that the primary dendritic skeleton has been completely refined to equiaxed grains. Compared with the first grain refinement, the equiaxed grains at this time have straight grain boundaries and smaller grain sizes. The grain boundaries have obvious migration and annealing twins exist in the solidified structure, which are consistent with recrystallization.

Through the systematic research on the microstructure evolution of Ni65Cu35 alloy, it is found that the morphology transformation of "coarse dendrite → circular equiaxedgrain → directional fine dendrite → hexagonal

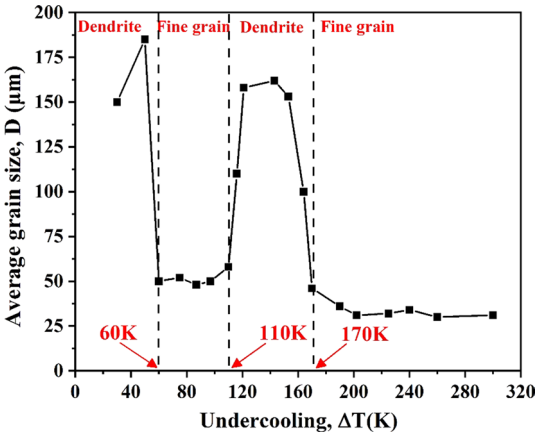

Fig. 4 Evolution of grain size of Ni65Cu35 alloys as a function of the initial undercooling

equiaxedgrain". In order to further compare the grain sizes of the two grain refinements, the average grain sizes at different undercoolings are obtained by drawing line method and measuring the length of the dendrite trunk, see Fig. 4. In the range of first grain refinement (70 K < ΔT < 110 K), the average grain size is reduced to about 50 μm, while in the range of second grain refinement (ΔT > 195 K), the average grain size is reduced to about 30 μm. Directional fine dendrites at high undercooling and coarse dendrites at low undercooling are similar in size. Compared with Ni80Cu20 and Ni90Cu10 alloys [5, 32], the overall grain size of Ni65Cu35 alloy at different undercoolings is smaller, which may be caused by the increase of the mass fraction of Cu.

The initial undercooling consists of four components. The BCT model [6, 44] describes the changes of various component undercoolings with the initial undercooling during dendrite growth, which can well explain the difference of dendrite morphology during solidification. According to this model, the initial undercooling during dendrite growth consists of the following four components:

$$\Delta T = \Delta T\mathrm{r} + \Delta Tc + \Delta Tk + \Delta Tt \tag{1}$$

ΔTr is curvature undercooling, ΔTc is solute undercooling, ΔTk is kinetics undercooling, and ΔTtis thermal undercooling. Each component undercooling can be expressed as:

$$\Delta\mathrm{Tt} = \frac{\Delta H_f}{C_p} I_V(P_t) \tag{2}$$

$$\Delta Tc = \frac{k_0 \Delta T_0 I_V(P_c)}{1-(1-k_0) I_V(P_c)} \tag{3}$$

$$\Delta Tk = \frac{V}{\mu} \tag{4}$$

$$\Delta Tr = \frac{2\Gamma}{R} \tag{5}$$

where, $P_t = VR/2\alpha_L$ and $P_c = VR/2D_L$. And the dendrite tip radius can be expressed as:

$$R = \frac{\Gamma/\sigma^*}{\frac{\Delta H_f}{C_p}\cdot P_t - \frac{m_0 C_0(1-k_0)}{1-(1-k_0)\cdot I_V(P_c)}\cdot P_c} \tag{6}$$

where, $\sigma^* = 1/4\pi^2$.

According to the BCT model and using the parameters in Table 1, the evolution of each component undercooling of Ni65Cu35 alloy with initial undercooling can be calculated, see Fig. 5. Since curvature and kinetics undercooling of Ni-Cu alloys have little effect on dendrite morphology, the analysis of solute undercooling and thermal undercooling was emphasized. It can be seen from Fig. 5 that when the undercooling is less than 70 K, the proportion of solute undercooling is large, and the solute diffusion controls the growth of dendrites in a narrow space. The microstructure is similar to the thick dendrite in the casting state, and contains significantly thick secondary dendrite arms. With the increase of undercooling, the proportion of thermal undercooling increases sharply. When ΔT > 110 K, it can be seen that the proportion of thermal undercooling is quite large. Thermal diffusion takes the leading role in controlling the dendrite growth process so that the dendrite growth proceeds in the direction of thermal diffusion. The microstructure is a developed directional fine dendritic network, see Fig. 3c–e.

Two grain refinements with quite different grain size and microstructure morphology occur in the solidification structure of Ni65Cu35 alloy at different undercoolings, which must correspond to the different mechanisms. Due to the superheat, the primary dendritesat low undercooling will remelt and refine into equiaxed grains. This conclusion can also be reflected from the solidification temperature curves shown in Fig. 2. For grain refinement at high undercooling, the stress-induced recrystallization mechanism [46] indicatesthat the rapid solidification can accumulate stress between the primary dendritic skeleton, and the plastic deformations occur when the stress exceeds the yield strength of the alloy. And the plastic strainsasthe thermodynamic driving force to promote recrystallization during the post-recalescence period. At present, the grain refinement at low undercooling has been widely interpreted as the dendrite superheat remelting. However, the stress-induced recrystallization at high undercooling remains to be further studied. In the following discussion, the characterization methods of EBSD, TEM and Microhardness are used to further explain it.

3.2 Grain Refinement Mechanism

The microstructure of Ni65Cu35 alloy was characterized by EBSD to further explain the grain refinement mechanism athighundercooling. For the grain refinement at highundercooling, the recrystallization mechanism indicates thatwhen the undercooling exceeds a certain critical value, the accumulated plastic strains in the microstructure as the driving force promote the low-angle grain boundaries to migrate to high-angle and recrystallization of structure [14, 47, 48]. To further reduce the interface energy, the grain boundaries become straight, and the microstructure is regular hexagonal equiaxed grains with annealing twins. EBSD can well identify the typical characteristics of these recrystallization, including high-angle grain boundaries, random orientation and annealing twins.

Figure 6 shows the EBSD characterization of Ni65Cu35 alloy at $\Delta T = 70$ K and320K. Fig. 6a–b are grain orientations and different colors correspond to different orientations [49, 50]. At low undercooling, there are many same or similar colors, and the grain orientations are roughly the same, see Fig. 6a. However, at high undercooling, the colorsare chaotic and the grain orientations aremore random. Here, the misorientation less than 15° is defined as the low-angle grain boundaries, and the rest is the high-angle. By comparing the misorientation distribution of the grain boundaries, it is clear that almost all the grain boundaries at lowundercooling are low-angle, see Fig. 6c. However, at highundercooling, the high-angle boundaries are as high as 90%, and the proportion of $\sum 3$ twin boundaries is as high as 20%, see Fig. 6d.

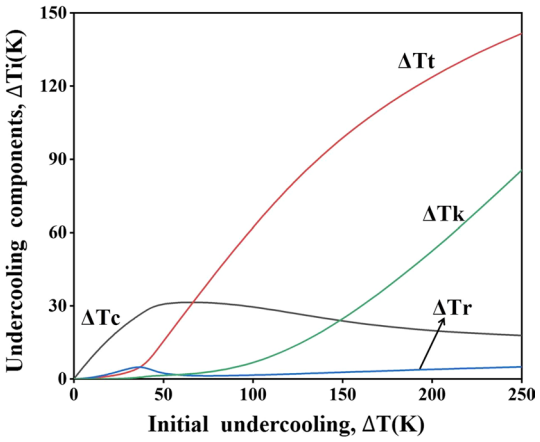

Fig. 5 Undercooling constituents as a function of initial undercoolings for Ni65Cu35 alloy

According to research on Ni–Cu alloys, stress accumulation and a small amount of dendrite remelting athighundercooling are random, and no new growth texture is introduced. By comparing the polar figure, it is found that there is no high-strength texture at high undercooling (max is 3.94, see Fig. 6f). However, the growth texture is more obvious at low undercooling (max is 37.49, see Fig. 6e). The grain orientation is randomly distributed at highundercooling, almost all of which are high-angle boundaries, and there are high-density annealing twins. Thispreliminarily indicate the grain refinement at high undercooling is caused by recrystallization. However, the grain orientationsare uniform

Table 1 Physical parameters used in the Calculation [19, 45]

Parameters	Value of Ni65Cu35 alloy
Heat of fusion ΔH_f/kJ mol^{-1}	17,160
Specific heat of the liquid C_p/J^{-1} mol^{-1} K^{-1}	38.5
Dynamic viscosity of the liquid μ/Pas	10^{-3}
Molar volume of the liquid V_m^L/m^3 mol^{-1}	8.06×10^{-6}
Molar volume of the solid V_m^S/m^3 mol^{-1}	7.08×10^{-6}
Liquidius T_L/K	1653 K(1380 ℃)
Solute diffusivity in the liquid D_L/m^2 s^{-1}	4×10^{-9}
Thermal diffusivity α_L/ m^2 s^{-1}	1.78×10^{-5}
Atomic space a_0/m	4×10^{-10}
Interfacial energy $\sigma_{S,L}$/J m^{-2}	0.36
Speed of sound in the melt V_0/m s^{-1}	4000
Equilibrium liquidus slope m_L/K (at. –%)$^{-1}$	2.668
Equilibrium solute partition coefficient k_0	1.308
Solidification time t_f/s	0.1
Size of the mushy zone a/m	0.01
Gibbs–Thomson coefficient Γ	3.25×10^{-7}
Solid fraction at the dendrite coherency point $f_S{}^{coh}$	0.15
Solidification shrinkage of the primary phase β	0.1215
Atomic diffusive speed V_D/ms^{-1}	25

at lowundercooling, almost all of them are low-angle grain boundaries, and there is no annealing twin. According to previous research, the dendrite remelting can form the similar growth orientation, so it is consistent with the above characterization of microstructure, see Fig. 6a, c and e.

According to recrystallization mechanism [33, 46], the increase of undercooling has accelerated the solidification velocity, and the solidification shrinkage and thermal strain generated in the microstructure can accumulate stress between the primary dendritic skeletons, and the higher the undercooling, the larger the stress. In order to calculate it qualitatively, the stress accumulation during the rapid solidification process of the alloy can be expressed as:

$$\sigma_S = \frac{160\mu \cdot |\vec{a}|}{(f_R^S)^2 t_f \lambda_2^2} \times \frac{(1-f_S(\vec{x}))}{f_S(\vec{x})} \left\{ |\vec{a}| \cdot \beta_S \left[f_S(\vec{x}) - f_{coh} + \frac{1}{(1-f_S)} - \frac{1}{(1-f_{coh})} + 2\ln\left[\frac{1-f_S(\vec{x})}{1-f_{coh}}\right] \right] - \frac{2(1+\beta_S)\alpha_{\text{ther}}\Delta T_0 \Delta T}{3G_S} Q\left[f_S(\vec{x})\right] \right\} \tag{7}$$

where, $Q\left[f_S(\vec{x})\right] = \int_{f_{coh}}^{f_S} \frac{f_S(\vec{x})}{f_l(\vec{x})^3} \left[f_S(\vec{x})^3 - f_{coh}(\vec{x})^3\right] df_S(\vec{x})$ (8)

The accumulated stress in the microstructure of the alloy becomes larger and larger, and the stress even increases linearly under the condition of highundercooling. Figure 7 is a schematic diagram of the relationship between the accumulated stresses during rapid solidification and the initial undercooling of Ni65Cu35 alloy based on stress accumulation model. Although the accumulated stress in the microstructure gradually increases, no dislocations and defectscaused by the accumulated stress are found in the TEM bright-field images of the microstructure at high undercooling, see Fig. 8a–b. There are no obvious traces of plastic strain in the microstructure and the grains are regular hexagonal equiaxed grains with straight grain boundaries (Fig. 8b). The annealing twinsappear in the microstructure at high undercooling,which hasthe typical twin diffraction pattern of FCC alloy, see Fig. 8c–d. The stress accumulated during rapid solidification at high undercooling is large, but the microstructure is a non-plastic strain matrix with almost no visible dislocation and slip defects. This further indicates that the stress and strain accumulated during rapid solidification are completely dissipated by the system at the later stage of solidification, which is the driving force for the recovery and recrystallization of the structure, resulting in grain refinement. This further confirms stress-induced recrystallization mechanism.

Microstructure at each undercoolings was further characterized by microhardness tester, see Fig. 9. At low undercooling ($70\ \text{K} < \Delta T < 110\ \text{K}$), the microstructure changes from coarse dendrites to refined structures (equiaxed and granular grains) due to dendrite remelting (Fig. 3b–c). In this process, due to the effect of fine-grain strengthening, the number of grain boundaries is increased, the movement of dislocations and defects is hindered, and the microhardness increases sharply. With the increase of undercooling, although the proportion of dendrite remelting decreases at intermediate undercooling, the accumulated stress in the microstructure starts to increase linearly, and the microhardness decreases slightly compared with lowundercooling, but the hardness is still very high compared with highundercooling, which can be observed from the range of $110\ \text{K} < \Delta T < 195\ \text{K}$ in the Fig. 9. When the undercooling continues to increase to exceed the critical value (195 K),the second grain refinement occurs in the structure,and the accumulated stress should have beenvery large, so the microhardness should have been very high. However, it can be found in Fig. 9 thatwhen$\Delta T > 195$ K, the microhardness decreases sharply, and a large number of equiaxed grains and energy-stable annealing twins occur in the microstructure. The high proportion of high-angle grain boundaries appears in the undercooled range of second grain refinement, and there is no high-strength growth texture (Fig. 6). The annealed twins of typical FCC alloy exist in the microstructure (Fig. 8c–d). All of these indicate that the stress accumulated and other defectsact as the driving force to promote the recrystallization of the microstructure during the post-recalescence period. Therefore, the recrystallization and the decrease of system energy are the reasons for the hardness change at high undercooling. This is similar to the annealing of cold-deformed metals, except that this process is spontaneous refinement without human involvement [33, 43]. It can also be seen from TEM characterization that the system energy is very low (no obvious dislocations and defects, see Fig. 8a–c) at high undercooling, which is also corresponding to the sharp decrease of microhardness. The characterizations of the hardness, EBSD and TEM canreliably confirm the grain refinement at high undercoolingis caused by stress-induced recrystallization.

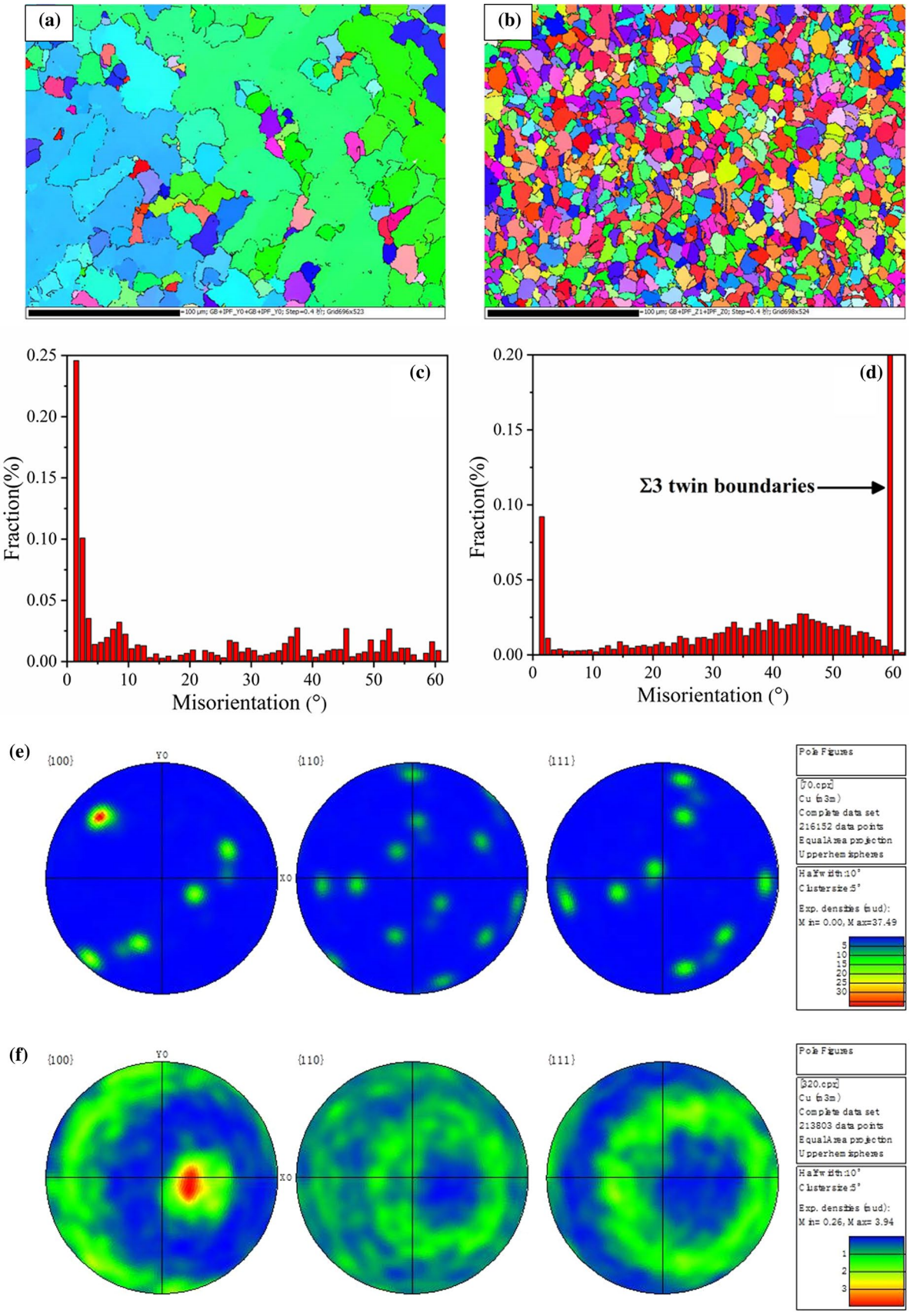
(a)
(b)
(c)
Fraction(%)
Misorientation (°)
(d)
Σ3 twin boundaries
Fraction(%)
Misorientation (°)
(e)
{100}
{110}
{111}
Y0
X0
Pole Figures
Cu (m3m)
Complete data set
216152 data points
Equal Area projection
Upper hemisphere
Halfwidth:10°
Cluster size:5°
Exp. densities (mud):
Min= 0.00, Max=37.49
(f)
{100}
{110}
{111}
Y0
X0
Pole Figures
Cu (m3m)
Complete data set
213803 data points
Equal Area projection
Upper hemisphere
Halfwidth:10°
Cluster size:5°
Exp. densities (mud):
Min= 0.26, Max= 3.94

◂**Fig. 6** **a** Grain orientation of Ni65Cu35 alloy at 70 K; **b** Grain orientation of Ni65Cu35 alloy at 320 K; **c** grain boundary misorientation distribution of **a**; **d** grain boundary misorientation distribution of **b**; **e** pole figure of **a**; **f** pole figure of **b**

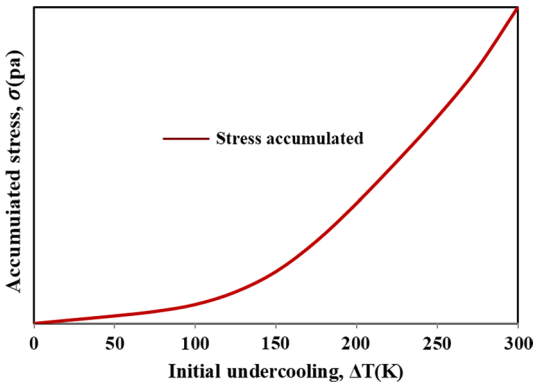

Fig. 7 Stress accumulated of Ni65Cu35 alloys during rapid solidification as a function of the initial undercoolings

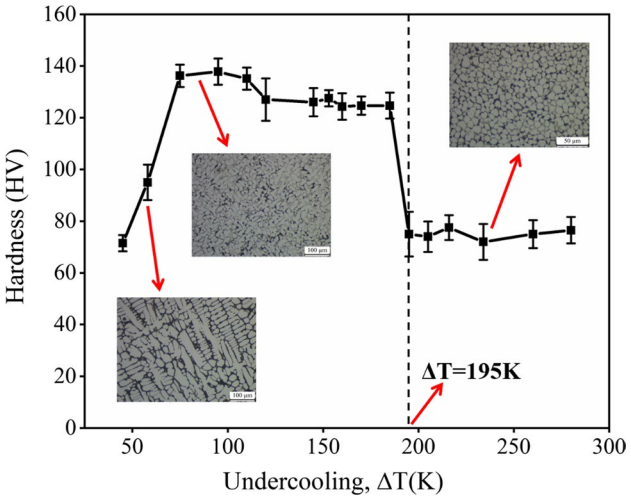

Fig. 9 Microhardness as a function of initial undercoolings for Ni65Cu35 alloy

Fig. 8 **a, b** TEM bright-field images of Ni65Cu35 alloy at 320 K. **c, d** The annealing twin and selected area electron diffraction pattern (SAED) of the twin boundary

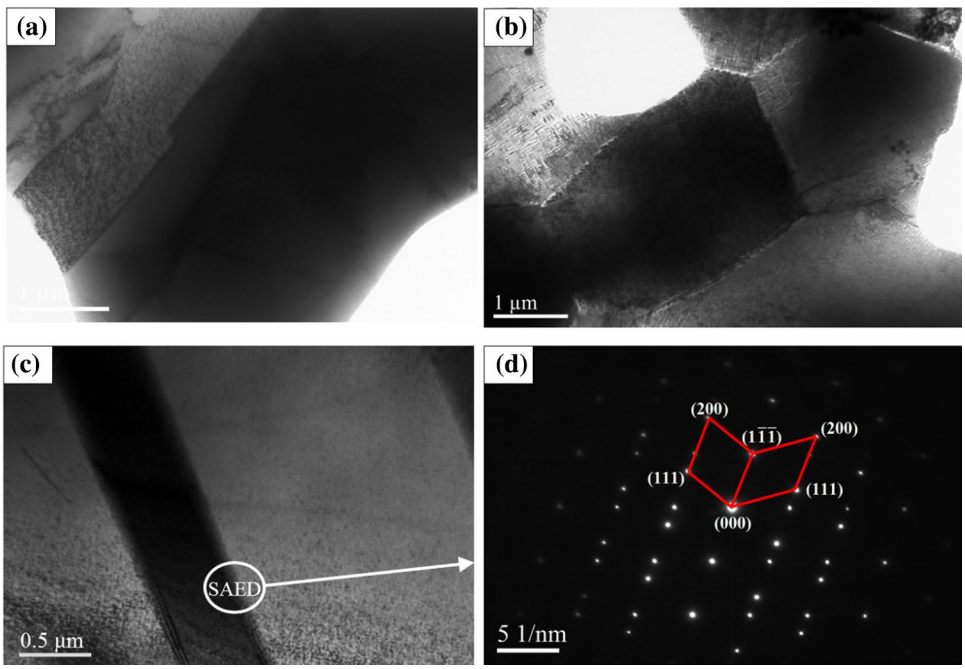

4 Conclusions

The maximum undercooling of Ni65Cu35 alloy has reached 320 K and the microstructure evolution was systematically analyzed. There were two grain refinements occurred atlow and highundercoolings. The solid-state structures at different undercoolings were further characterized by EBSD, TEM and microhardness tester, and the grain refinement mechanism was further explained by combining the stress accumulation model. The conclusions reached are as follows:

(1) Ni65Cu35 alloy has two grain refinements in the undercooling range. The first grain refinement occurs in the range of 70 K < ΔT < 110 K withthe microstructure of circular equiaxed grains. The second grain refinement occurs in the range of ΔT > 195 K, the microstructure is hexagonal equiaxedgrains with straight grain boundaries, which are filled with annealing twins. Moreover, the grain size of grain refined athighundercooling is smaller than that in lowundercooling.

(2) The microstructure at high undercooling has high-density $\sum 3$ twin grain boundaries and high-angle grain boundaries, with strongly random growth orientation. This is the important evidences of recrystallization. The grain orientations are uniform at low undercooling and almost all of them are low-angle, which are consistent with the dendrite superheat remelting.

(3) With the increase of undercooling, the accumulated stress in the microstructure increases gradually increases linearly. However, no plastic strains due to stress was found in the refined structure, and typical twins of FCC alloy existed. The microhardness decreases sharply after criticalundercooling. All these further confirm that it's the recrystallization causes the grain refinement at high undercooling.

Funding This work is supported by the National Natural Science Foundation of China (Nos.51701187, 51804279, 51774254), The Science and Technology Major Project of Shanxi Province (No. MC2016-06). Basic Applied Research Projects in Shanxi Province (201801D221151). Science and technology innovation project of colleges and universities in Shanxi Province in 2019 (2019L0528).

References

1. D.M. Herlach, Mater. Sci. Eng. R. Rep. **12**, 177 (1994)
2. H. Hou, Y. Li, X. Xu, Y. Zhao, F. Liu, Mater. Sci. Technol. **34**, 402 (2018)
3. R. Dong, J. Li, H. Kou, J. Fan, Y. Zhao, H. Hou, L. Wu, J. Mater. Sci. Technol. **44**, 24 (2020)
4. X.L. Xu, Y.Z. Chen, F. Liu, Mater. Sci. Technol. **28**, 1492 (2012)
5. K. Ma, Y. Zhao, X. Xu, H. Hou, J. Cryst. Growth **513**, 30 (2019)
6. Y. An, L. Liang, X. Xu, Y. Zhao, H. Hou, J. Marter. Res. **11**, 548 (2021)
7. Y. An, X. Xu, L. Liang, Y. Zhao, H. Hou, J. Alloy. Compd. **864**, 158821 (2021)
8. K. Wang, H. Wang, F. Liu, H. Zhai, Acta Mater. **61**, 4254 (2013)
9. W. Yang, F. Liu, H.F. Wang, Z. Chen, G.C. Yang, Y.H. Zhou, J. Alloy. Compd. **470**, L13 (2009)
10. T. Zhang, F. Liu, H.F. Wang, G.C. Yang, Scripta Mater. **63**, 43 (2010)
11. M. Hedayatian, K. Vahedi, A. Nezamabadi, A. Momeni, Met. Mater. Int. **26**, 760 (2020)
12. C.D. Lee, C.S. Kang, K.S. Shin, Met. Mater. Int. **6**, 351 (2000)
13. B. Nayebi, M. Mehrabian, A. Bahmani, D. Dietrich, M. Shokouhimehr, Met. Mater. Int. **27**, 1701 (2021)
14. X.L. Xu, F. Liu, H. Hou, Y.H. Zhao, T. Gu, S.Y. Wang, F. Yan, J. Cryst. Growth **455**, 29 (2016)
15. X.L. Xu, F. Liu, Cryst. Growth Des. **14**, 2110 (2014)
16. J.F. Li, W.Q. Jie, G.C. Yang, Y.H. Zhou, Acta Mater. **50**, 1797 (2002)
17. J.F. Li, Y.C. Liu, Y.L. Lu, G.C. Yang, Y.H. Zhou, J. Cryst. Growth **192**, 462 (1998)
18. J.F. Li, Y.H. Zhou, G.C. Yang, J. Cryst. Growth **206**, 141 (1999)
19. S.Y. Lu, J.F. Li, Y.H. Zhou, J. Cryst. Growth **309**, 103 (2007)
20. M. Satyanarayana, K. Adepu, K. Chauhan, Met. Mater. Int. **27**, 3563 (2021)
21. L. Wang, J. Jiang, B. Saleh, R. Fathi, H. Huang, H. Liu, A. Ma, Met. Mater. Int. (2021). https://doi.org/10.1007/s12540-020-00958-5
22. P. Zhang, H. Wang, S.J. Yao, C.J. Wang, Q. Zhu, G. Chen, Met. Mater. Int. **27**, 392 (2021)
23. B. Hamrahi, A. Khanlarkhani, S.M. Madani, A. Fattah-Alhosseini, S.O. Gashti, Met. Mater. Int. (2020). https://doi.org/10.1007/s12540-020-00736-3
24. E. Maleki, G. H. Farrahi, K. R. Kashyzadeh, O. Unal, M. Gugaliano, S. Bagherifard, Met. Mater. Int. **27**, 2575 (2021)
25. S. Shahriyari, S. Pashmforoosh, O. Mirzaee, Met. Mater. Int. **27**, 4250 (2021)
26. F. Liu, X. Guo, G. Yang, Mater. Sci. Eng. A **300**, 190 (2001)
27. X. Xu, Y. Zhao, H. Hou, F. Liu, J. Alloy. Compd. **744**, 749 (2018)
28. X.L. Xu, Y.Z. Chen, F. Liu, J. Cryst. Growth **377**, 153 (2013)
29. X.L. Xu, Y.Z. Chen, F. Liu, Mater. Sci. Technol. **29**, 117 (2013)
30. Y. An, X. Xu, Y. Zhao, H. Hou, J. Alloy. Compd. **881**, 160658 (2021)
31. H. Wang, F. Liu, G. Yang, J. Mater. Res. **25**, 1963 (2011)
32. X.L. Xu, F. Liu, J. Alloy. Compd. **597**, 205 (2014)
33. X.L. Xu, F. Liu, J. Alloy. Compd. **615**, 156 (2014)
34. Z. Chen, T. Liang, Y. Zhang, L.C. Feng, X.Q. Yang, Y. Fan, Mater. Charact. **127**, 73 (2017)
35. Y. Lu, F. Liu, G. Yang, H. Wang, Y. Zhou, Mater. Lett. **61**, 987 (2007)
36. X. Xu, Y. Zhao, H. Hou, F. Liu, Int. J. Mater. Res. **109**, 593 (2018)
37. H. Wang, Y. An, X. Xu, X. Guo, Y. Hu, Mater. Charact. **170**, 110703 (2020)
38. K.I. Dragnevski, R.F. Cochrane, A.M. Mullis, Mater. Sci. Eng. A **375–377**, 479 (2004)
39. M. R. Rahul, G. Phanikumar, J. Alloy. Compd. **815**, 152334 (2020)
40. M. R. Rahul, G. Phanikumar, Mater. Sci. Eng. A **777**, 139022 (2020)
41. M.R. Rahul, S. Samal, A. Marshal, V.I.N. Balaji, K.G. Pradeep, G. Phanikumar, Scripta Mater. **177**, 58 (2020)
42. X.L. Xu, Y.H. Zhao, H. Hou, Mater. Sci. Technol. **35**, 900 (2019)
43. E.G. Castle, A.M. Mullis, R.F. Cochrane, Acta Mater. **77**, 76 (2014)
44. N. Liu, G. Yang, F. Liu, Y. Chen, C. Yang, Y. Lu, D. Chen, Y. Zhou, Mater. Charact. **57**, 115 (2006)
45. J. Zhang, Y. Zhang, F. Zhang, D. Cui, Y. Zhao, H. Wu, X. Wang, Q. Zhou, H. Wang, J. Alloy. Compd. **816**, 152529 (2020)
46. N. Liu, F. Liu, G. Yang, Y. Chen, D. Chen, C. Yang, Y. Zhou, Phys. B **387**, 151 (2007)
47. X.L. Xu, Y.H. Zhao, H. Hou, J. Alloy. Compd. **773**, 1131 (2019)
48. F. Zhang, H.-F. Wang, C. Lai, J.-B. Zhang, Y.-C. Zhang, Q. Zhou, T. Nonferr. Metal. Soc. **30**, 1826 (2020)
49. J. Zhang, H. Wang, F. Zhang, X. Lü, Y. Zhang, Q. Zhou, J. Alloy. Compd. **781**, 13 (2019)
50. X. Xu, H. Hou, Y. Zhao, F. Liu, Mater. Sci. Technol. **34**, 79 (2018)